Biochimica et Biophysica Acta 1861 (2017) 1515–1520

Contents lists available at ScienceDirect

Biochimica et Biophysica Acta

journal homepage: www.elsevier.com/locate/bbagen

Iron oxide nanoparticle surface decorated with cRGD peptides for magnetic resonance imaging of brain tumors☆

Sophie Richard [a], Marianne Boucher [b], Yoann Lalatonne [c,d], Sébastien Mériaux [b], Laurence Motte [d,*]

[a] Laboratoire Matière et Systèmes Complexes (MSC), UMR 7057, CNRS and Université Paris Diderot, 75205 Paris Cedex 05, France
[b] Unité d'Imagerie par Résonance Magnétique et de Spectroscopie, CEA/DRF/I2BM/NeuroSpin, F-91191, Gif-sur-Yvette, France
[c] Service de Médecine Nucléaire, Hôpital Avicenne Assistance Publique-Hôpitaux de Paris, F-93009 Bobigny, France
[d] Inserm, U1148, Laboratory for Vascular Translational Science, UFR SMBH, Université Paris 13, Sorbonne Paris Cité, F-93017 Bobigny, France

ARTICLE INFO

Article history:
Received 30 September 2016
Received in revised form 7 December 2016
Accepted 19 December 2016
Available online 23 December 2016

Keywords:
Glioblastoma
Iron oxide nanoparticle
MRI contrast agent
cRGD
Targeting

ABSTRACT

In this article, a specific targeting Magnetic Resonance Imaging (MRI) nanoplatform, composed by iron oxide nanoparticle (NP) with cRGD peptides as targeting agent onto NP surface, is explored for the diagnosis of brain tumors by MRI using intracranial U87MG mice xenograft tumor. This article is part of a Special Issue entitled "Recent Advances in Bionanomaterials" Guest Editor: Dr. Marie-Louise Saboungi and Dr. Samuel D. Bader.

1. Introduction

Since the last 30 years, new techniques for imaging are increasingly used in order to understand in particular the complexity of the *in vivo* behavior of cancers. With all advances in this domain, a new imaging category is expending: the molecular imaging which consists to target molecular ligand over-expressed on tumor cell surface. The aims are to identify *in vivo,* and through non invasive imaging techniques, the pathology as well as with an early stage disease diagnostic, and also to try to quantify the extent of the disease in order to optimize the specific therapeutic treatment for a patient (personalized medicine), and finally to track the effectiveness of this specific treatment [1–3]. Thus, many challenges remain to be improved concerning imaging technologies as well as related to the elucidation of pertinent biomarkers for imaging tracing and in order to develop new contrast agent dedicated to a specific pathology [4,5].

Nanomedicine represents a set of interdisciplinary research at the interface between biology, physics and chemistry. It allows considering various and relevant applications for research against cancer, comprising the development of nano-carriers for targeted delivery of anticancer drugs and imaging contrast agents. Among these nanoparticles (NPs), iron oxide NPs are certainly the most promising material for medical applications. Due to their magnetic intrinsic properties, these NPs increase the Magnetic Resonance Imaging (MRI) signal and improve the tumor detection. In addition, their good biodegradability and NP surface modification with molecules for targeting or therapy, represents an important advantage for applications in the field of diagnosis, prevention, therapy and personalized medicine [6,7].

In oncology area, gliomas, although classified as a rare disease, are a major problem of neuro-oncology due to the severity of this pathology and the difficulty to treat it [8]. Gliomas are the most common cancers of the central nervous system and represent 30% of primary and malignant brain tumors [9,10]. Glioblastoma, or glioblastoma multiform (GBM), represents around 65% of gliomas and is the most aggressive gliomas [9]. These tumors have a very rapid and invasive growth. Current treatments of GBM include a surgical resection followed by radiotherapy and chemotherapy. The only surgical resection provides a median survival of approximately 6 months. When the latter is coupled to the radiotherapy, the median survival was increased to 12.1 months. Finally, the addition of chemotherapeutic agents, in addition to surgical resection and radiation therapy, increases the median survival to 14.6 months [11]. Nevertheless, treatments are ineffective due to the high number of recurrences. This is why many researches are trying to target these tumors more specifically.

One of these strategies is to target the angiogenesis process which is one of the characteristics of tumor tissues. This approach is particularly

☆ This article is part of a Special Issue entitled "Recent Advances in Bionanomaterials" Guest Editor: Dr. Marie-Louise Saboungi and Dr. Samuel D. Bader.

* Corresponding author.
E-mail address: laurence.motte@univ-paris13.fr (L. Motte).

http://dx.doi.org/10.1016/j.bbagen.2016.12.020
0304-4165/

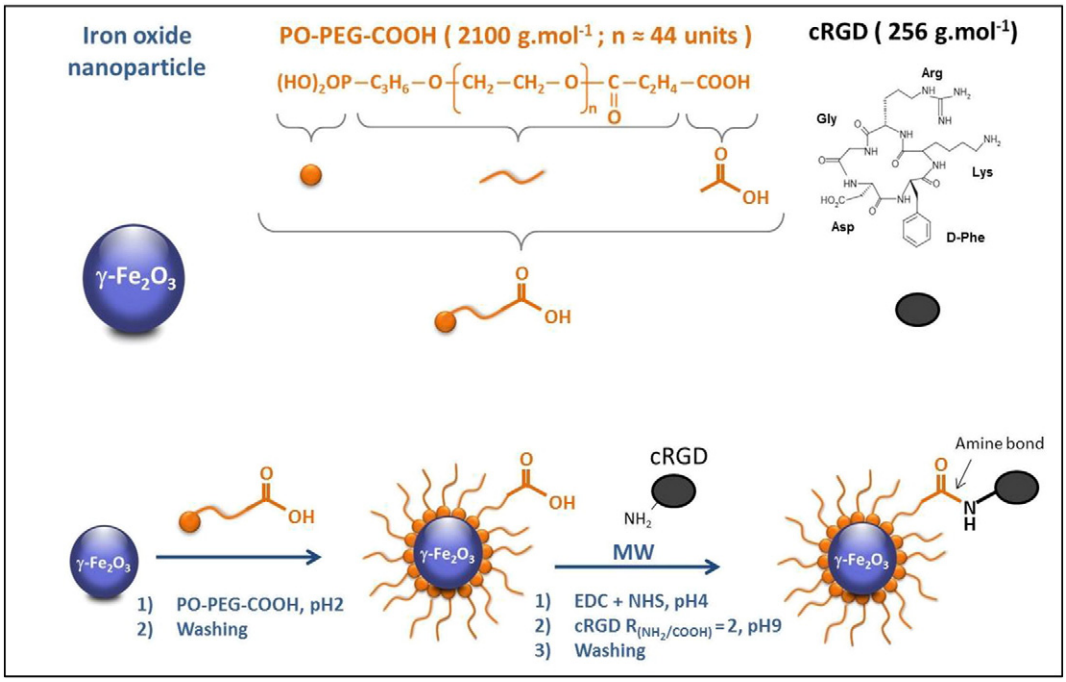

Fig. 1. Schema of the different steps for the synthesis of nanoplatforms.

interesting in the case of the GBM because this cancer is among the most highly vascularized tumor [12,13].

In this approach, $\alpha v\beta_3$ integrin appears as a pertinent target because integrin plays an important role in angiogenesis, pathological neovascularization and in the development of tumors metastases [14]. The $\alpha_v\beta_3$ integrin expression in cancer cells is well correlated with the progression of various types of tumors such as melanomas, breast cancer, prostate cancer, ovarian cancer or glioblastomas. In this latter case, a better mobility and cellular resistance to apoptosis was observed. Therefore integrins appears to be a relevant target for imaging contrast agents diagnosis as well as for drugs delivery in order to regulate the migration, growth and tumor cell differentiation and apoptosis. Hence the targeting of integrin could be at the origin of the design of new treatments for diseases such as thrombosis, osteoporosis and cancer [15–17].

Various tumor targeting molecules are explored including antibodies, peptides or oligonucleotides [18–21]. Considering $\alpha_v\beta_3$ integrin targeting, various studies have identified a peptide sequence (aspartic acid-glycine-arginine, or RGD) for this specific recognition [22]. RGD has been recognized as the minimal sequence required for binding to integrin $\alpha_v\beta_3$ but also with other known integrins including $\alpha_{IIb}\beta_3$, $\alpha_5\beta_1$, $\alpha_v\beta_5$ and $\alpha_v\beta_6$ [23]. Thus, this peptide sequence is considered as a model molecule for targeting integrins. The sequence and structure of the RGD motif peptides could be cyclic or linear. However, cyclic RGD peptides, or cyclo RGD (cRGD) have exhibited superior activity compared to linear RGD peptides [24,25]. Besides the hyperpermeable nature of the tumor vessels leads to a blood–brain barrier (BBB) leakage, and this very aggressive pathology induces a loss of junction between the endothelial cells composing the BBB [26–28].

Hence, potential strategy for glioblastoma diagnosis is related to the development of a MRI contrast agent coupled to a cRGD peptide sequence in order to target the $\alpha v\beta_3$ integrin and to obtain an early diagnosis of tumor or pathologic neovascularization using MRI.

Here, iron oxide nanoparticles, potential MRI contrast agents do to their inherent magnetic physical properties, were surface functionalized with phosphonate PEG chains and covalently coupled to cRGD by carbodiimide chemistry assisted with microwave. Several chemico-physical techniques were used to characterize the nanoplatform. Finally, *in vivo* experiments were performed using intracranial glioblastoma tumor xenograft mice in order to evaluate the potent of these NPs as MRI contrast agent.

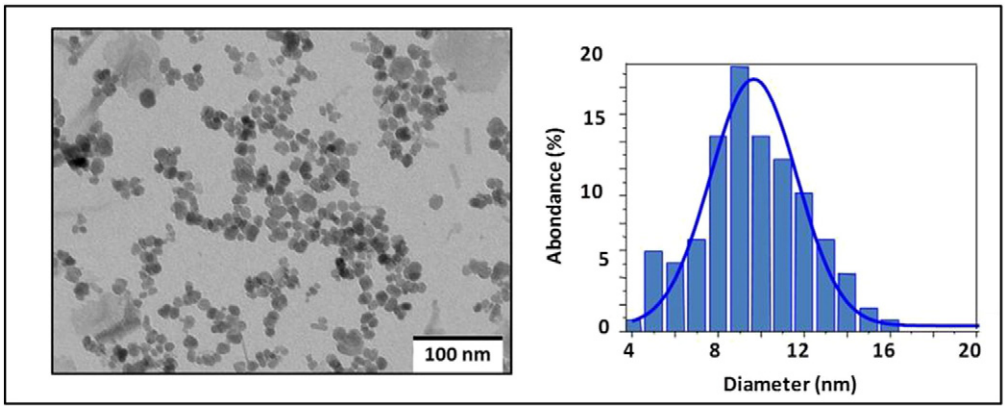

Fig. 2. NP size distribution and TEM image.

2. Experimental

2.1. Materials

Reagents for NP synthesis were from Sigma-Aldrich (Saint Louis, MO, USA). Phosphonate- poly(ethylene glycol) PO-PEG-COOH (MW 2100 g·mol^{-1}; n ≈ 44 units) were purchased from Specific Polymers (Specific polymers, ref. SP-1P-10-002, Castries, France). Cyclo(Arg-Gly-Asp-d-Phe-Lys) (cRGDfK or cRGD) was purchased from Acros.

2.2. Synthesis of γFe_2O_3@PO-PEG-cRGD NPs

Non coated maghemite γFe_2O_3 NPs were synthesized by the reaction of ferrous dodecyl sulfate with dimethylamine as previously described [29]. Briefly, dimethylamine ($(CH_3)_2NH_2OH$) was added to an aqueous solution of ferrous dodecyl sulfate ($Fe(DS)_2$) The final concentrations after the reactants mixed were 2.7×10^{-2} mol·L^{-1} and 2.8×10^{-1} mol·L^{-1} for $Fe(DS)_2$ and dimethylamine, respectively. Then the solution was stirred vigorously for 2 h at 28.5 °C. Finally, the solution was rinsed under acidic conditions using 2 mL of HCl (1 M) in order to reach the isoelectric point (around pH 7), inducing NPs precipitation. The precipitate was isolated from the supernatant using magnetic separation. The magnetic NPs were then separated from the supernatant using a permanent magnet and washed 10 times at neutral pH. The NPs were then dispersed at pH 2 in distilled water (adjusted with HCl solution).

To coat the NPs with PO-PEG-COOH (MW = 2100 g·mol^{-1}; n ≈ 44 units), both compounds were mixed during 2 h at pH 2 with a mass (PO-PEG-COOH/NP) ratio equal to 10. After washing procedure using ultrafiltration process (Amicon 30 kDa, Merck Millipore) in order to remove excess molecules, the magnetic γFe_2O_3@PO-PEG-COOH NPs were then dispersed in distilled water and the pH adjusted to 7.4.

The coupling of the cRGD peptide onto the γFe_2O_3@PO-PEG-COOH NPs was performed in water assisted by microwaves [30,31]. The first step is the activation of the carboxylic acid functions at the outer surface of the NPs using 1-ethyl-3-(3-dimethylaminopropyl) carbodiimide (EDC, $n_{EDC} = 5n_{COOH}$) and N hydroxysuccinimide (NHS, $n_{NHS} = 5n_{COOH}$) at pH 4. The second step is the conjugation of the amine function of the cRGD peptide with the activated carboxylic acid functions of the pegylated chains surrounding nanocrystals. The reaction was performed at pH 9 (adjusted with N,N-diisopropylethylamine) with a molar ratio $R = n_{COOH}/n_{NH2} = 2$, Fig. 1. The γFe_2O_3@PO-PEG-cRGD NPs were isolated with a magnet at pH 2 (using HCl solutions) and washed several times with deionized water. The particles were re-dispersed at pH 7.4 in distilled water for various physicochemical characterizations.

2.3. Characterization techniques

2.3.1. TEM analysis

TEM images were obtained using a FEI CM10 microscope (Philips), and samples were prepared by depositing a drop of NPs suspension on carbon-coated copper grids placed on a filter paper. The median diameter is deduced from TEM data measurements, simulating the diameter distribution with a log-normal function.

2.3.2. Hydrodynamic properties

The hydrodynamic size and zeta potential of the various nanoplatforms ([Fe] = 0.25 mM, pH = 7) were investigated by dynamic laser light scattering, measuring, using a Nano-ZS (632.8 nm) ZEN 3600 device (Malvern Instruments, Malvern, UK).

2.3.3. Infra-red spectroscopy

The grafting of the molecules to the surface of the various platforms was studied by Fourier transform infra-red (FTIR) analysis. The FTIR spectra were recorded as thin films on KBr pellets on a Thermo Scientific Nicolet 380 FTIR and are reported in wavenumbers (cm^{-1}).

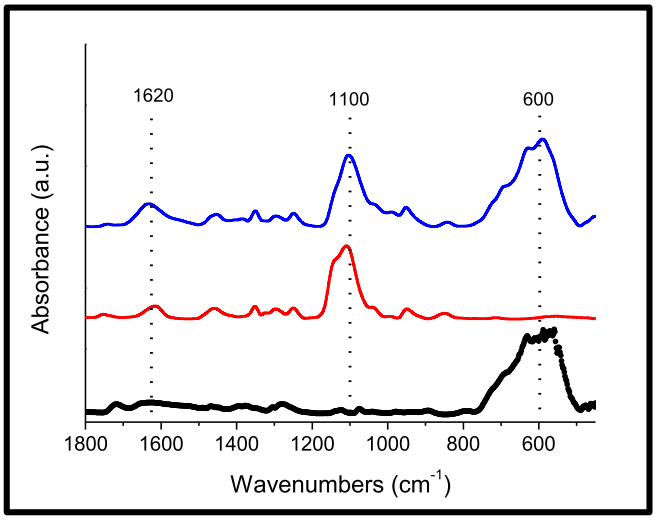

Fig. 3. Infrared spectrum of the uncoated NPs (black), free molecules PO-PEG-COOH (red) and γFe_2O_3@PO-PEG-COOH NPs (blue). The spectra were normalized with the Fe–O vibration band at 600 cm^{-1}.

2.3.4. Quantitation

Quantitation of PO-PEG-COOH coating and grafting per particle was evaluated by EDX. EDX microanalyses were performed using a TM 3000 tabletop microscope equipped with a Swift EDX-ray 3000 microanalysis system (Oxford Instruments). Samples were deposited as powder on a copper surface, and data were collected using a 15 kV accelerating voltage, studying ratio of iron versus phosphorus. The maghemite density, equal to 4.9 g.cm^{-3}, is used to determine the mass of 9.6 nm NP. Then the average number of iron atoms/particles is deduced with the maghemite molecular weight, equal to 160 g.mol^{-1}.

The average number of grafted cRGD per nanocrystal was deduced using the OPA (o-Phtalaldehyde and 2-mercaptoéthanol) reagent. The OPA reacts with amines to form blue fluorescent isoindoles in the presence of reduced thiols. The amount of grafted cRGD per nanoparticle was deduced after chemical decomposition (2 N NaOH, 60 °C, overnight) of the coupling and titration of amino groups in the supernatant. To do this quantification, 50 μL of the sample was diluted in 50 μL of 2 M NaOH and left overnight at 60 °C. Then, 900 μL of OPA reagent was added to the mixture and fluorescence was measured at 595 nm (λ_{ex} = 330 nm). The fluorescence measurements were performed

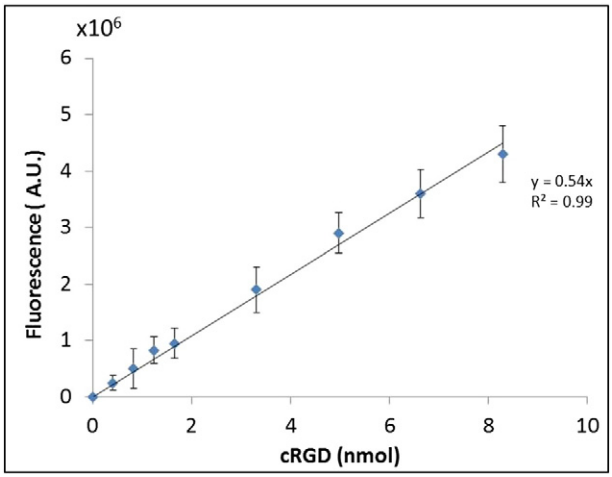

Fig. 4. Calibration curve of cRGD by fluorescent measurement with the OPA method.

Table 1
Hydrodynamic diameter and zeta potential of the γFe_2O_3@PO-PEG-COOH and γFe_2O_3@PO-PEG-cRGD NPs.

cRGD/NP	D_H (nm)	Zeta (mV)
0	14.7 ± 4.4	−20.4 ± 7.7
17 ± 9	38.9 ± 9.3	−23.9 ± 4.6

with a Spex Fluoro Max spectrofluorometer (HORIBA Jobin–Yvon, France) equipped with a Hamamatsu Photonics K.K. 928 photomultiplier (Hamamatsu, Japan). For each experiment, a calibration curve was plotted.

2.4. Relaxivities measurements

Transverse relaxivities r_2 of γFe_2O_3@PO-PEG and γFe_2O_3@PO-PEG-cRGD NPs were measured *in vitro* at 37 °C and 11.7 T (Bruker PharmaScan preclinical scanner, Ettlingen, Germany) using dedicated phantoms consisting of 6 tubes filled with different concentrations of contrast agent (from 0.001 to 0.04 mM) suspended in 0.3% w/w agar matrix. T_2 parametric maps were acquired with a Multi-Slice Multi-Echo sequence (TE = 7.7 ms, 64 echoes, TR = 10.000 ms, Field Of View = 3 × 3 cm^2 in-plane, acquisition matrix = 120 × 120, 6 slices of 1.25 mm thickness, total acquisition time = 1 h 20 min).

In a first post-processing step, T_2 parametric maps were reconstructed by fitting the signal intensity versus echo time using Bloch equations. Then, the mean proton relaxation rate R_2, equal to the inverse of relaxation time T_2, was computed for each tube, and a linear fit of R_2 values versus iron concentrations was performed to estimate the transverse relaxivity r_2 as the slope of the fitted curve.

2.5. In vivo MR imaging of xenografted U87MG tumor model

2.5.1. Intracranial tumor xenograft model

All *in vivo* experiments were conducted in strict accordance with the recommendations of the European Community (2010/63/EU) and the French legislation (decree no. 2013-118) for use and care of laboratory animals. The protocol for contrast agent injection has been approved by the Comité d'Éthique en Expérimentation Animale du Commissariat à l'Énergie Atomique et aux Energies Alternatives – Direction des Sciences du Vivant Ile-de-France (CETEA/CEA/DSV IdF) under protocol ID 12-058. U87-MG cells were cultured and amplified in DMEM supplemented with 10% of fetal bovine serum, 1% of glutamine, 1% of pyruvate, 1% penicillin/streptomycin, 7 μL/100 mL of gentamicin. Brain tumors were induced by intracerebral injection of U87-MG cells (60×10^6 cells in 2 μL) in athymic immunodeficient nude mice (NU/NU, Janvier, France). For the surgery, 5 weeks old male mice were anesthetized with an intraperitoneal injection of Ketamine/Xylazine (100/10 mg·kg^{-1}, 10 mL·kg^{-1}) and placed in a stereotaxic frame. A 1 mm hole was drilled in the skull 2 mm right to the bregma, and then U87-MG cells suspended in PBS were injected with a Hamilton syringe at 3.5 mm deep. The imaging session started around 2–3 weeks after implantation, when the tumor diameters were between 2 and 5 mm.

2.5.2. MRI experiments

MRI acquisitions were performed on an 11.7 T preclinical scanner equipped with a radiofrequency cryogenic coil dedicated to mouse brain (Bruker, Ettlingen, Germany) in order to maximize the detection of T_2^* effect induced by iron oxide nanoparticles. Mice were anesthetized using an air/O_2 mixture (50:50) and isoflurane (1–3%), before being positioned into dedicated cradle. Respiration rate was continuously monitored and body temperature was kept constant at 37 °C thanks to a warm water circulation system. Injection of 200 μmol[Fe]/kg of NP suspension was performed at the caudal vein with a 30 G needle while keeping the mouse positioned in the cradle. To visualize the biodistribution of injected NPs, a T_2^*-weighted FLASH (Fast Low Angle SHot) sequence was used with the following parameters: TE/TR = 8/1600 ms, 1 average, in-plane field-of-view = 1.92 × 1.47 cm^2, in-plane resolution = 75 × 75 μm [2], 90 slices of 75 μm thickness, total acquisition time = 5 min. MR images were reconstructed from raw data using a homemade pipeline consisting of Matlab routines (MathWorks, Natick, USA).

3. Results

3.1. NP characterization

Transmission electron microscopy (TEM) was used to examine the γFe_2O_3@PO-PEG NP morphology, Fig. 2. The NPs had a spherical shape, and a crystalline size about 9.6 nm was determined. Simulating the diameter distribution with a lognormal function, a standard deviation of 0.2 was deduced.

Infrared spectroscopy was used to study the complexation of PO-PEG-COOH on the NP surface, Fig. 3.

The uncoated NPs are characterized by the Fe–O vibration band at 600 cm^{-1} (black curve). Free PO-PEG-COOH molecules (red curve, Fig. 3) are mainly characterized by the intense ethylene oxide vibration band at 1100 cm^{-1} and the carboxylate symmetric vibration band at 1620 cm^{-1} The intense ethylene oxide vibration band overlay with the characteristic phosphonate asymmetric band which should appear between 1000 and 1200 cm^{-1} [32]. Nevertheless after the grafting of PO-PEG-COOH onto NPs surface, (ultrafiltration process was used in order to remove excess molecules), the PO-PEG-COOH characteristic bands at 600 cm^{-1}, 1100 cm^{-1} and 1620 cm^{-1} are still observed. This result clearly indicates the presence of the PO-PEG-COOH at the surface of the iron oxide nanoparticles.

EDX analysis was used in order to quantify the grafting. Considering that average NP diameter was 9.6 nm corresponding to an average

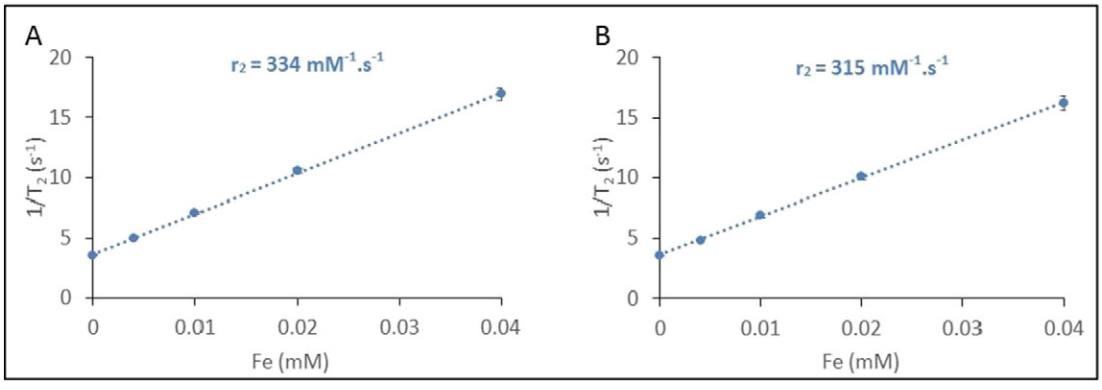

Fig. 5. *In vitro* transversal relaxivities measurements at 11.7 T of γFe_2O_3@PO-PEG-COOH (A) and γFe_2O_3@PO-PEG-cRGD (B).

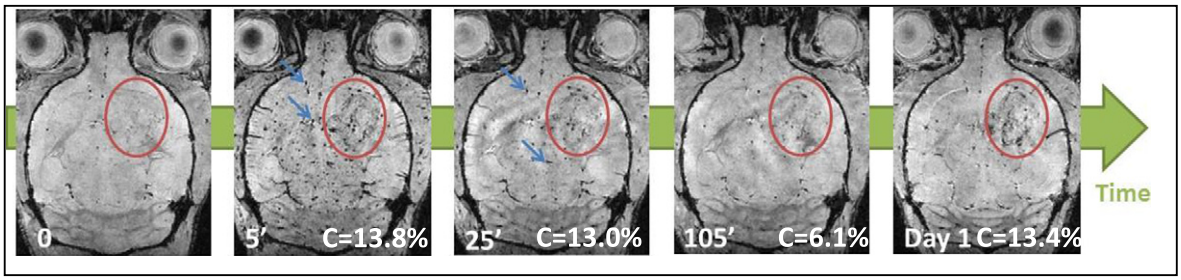

Fig. 6. FLASH images after γFe_2O_3@PO-PEG-cRGD injection. Insert: time after injection and contrast enhancement (C) observed between the tumoral region and contralateral healthy region computed after manual segmentation of the cerebral tumor. The tumoral zones indicated with red circles were manually segmented on RARE anatomical images.

number of iron atoms/NP equal to 15,800, the EDX ratio of iron versus phosphorus indicate an average of 583 ± 85 PO-PEG-COOH chains per NP. This result corresponds to a surface area of 0.5 nm^2 for each PO-PEG-COOH molecules, i.e. 2 PEG chain/nm^2. This surface area is in good agreement to the results obtained previously by surface modification of oxide nanomaterials with phosphonate moieties [33–35].

The amine function of cRGD peptide was used to covalently link cRGD on the γFe_2O_3@PO-PEG-COOH under microwaves. Indeed it was shown in previous work that in our conditions, microwaves allowed to enhance grafting yield compared to conventional heating [34]. The average number of cRGD ligand grafted per nanoparticle was deduced using OPA titration after chemical decomposition of the amide coupling onto NPs and using a calibration curve (Fig. 4).

With this method, around 17 cRGD grafted per nanoparticles were deduced. The efficiency of this coupling was also confirmed by Dynamic light scattering (DLS) measurements, Table 1. The hydrodynamic diameter of the γFe_2O_3@PO-PEG-COOH and γFe_2O_3@PO-PEG-cRGD nanoparticles were 14.7 ± 4.4 nm and 38.2 ± 9.3 nm respectively while the zeta potential remains similar. These variations of hydrodynamic diameter confirm the cRGD grafting.

The γFe_2O_3@PO-PEG-COOH NPs superparamagnetic behaviour induces a strong modification on the transverse nuclear relaxation times, T_2. To evaluate these NPs as MRI contrast agents, the transverse nuclear relaxation times, T_2, were measured on a 11.7 T preclinical MR scanner at room temperature for various iron concentrations suspended in an agar matrix (Fig. 5).

The transverse r_2 relaxivities were deduced from the slope of this curve and were equal to 334 and 315 $mM_{(Fe)}^{-1} \cdot s^{-1}$ for the γFe_2O_3@PO-PEG-COOH and γFe_2O_3@PO-PEG-cRGDNPs respectively. The high transversal relaxivities (r_2) confirmed the potential of these NPs as T_2-shortening contrast agents.

3.2. In vivo MRI acquisitions

In this work, we want to explore the active targeting using orthotopic U87-MG tumor, implanted in nude mouse brain. The γFe_2O_3@PO-PEG-cRGD NPs (200 μmol[Fe]/kg) were injected in the caudal vein to U87-MG mice and MR images of mouse brain were acquired before and after injection using a 11.7 T preclinical scanner. The ability of these NPs to be used as *in vivo* MRI nanoprobes is illustrated in Fig. 6.

An increase in the number of detected hypo-intense voxels was clearly observed 5 min after NP injection (blue arrow, Fig. 6). These results show that the NPs are circulating throughout the brain vascularization and generate a significant MRI contrast. This phenomenon is more important in the tumor area (red circle, Fig. 6) probably due to neoangiogenesis. These results confirm the efficiency of these NPs to circulate in the bloodstream. After 105 min a decrease of the number of hyposignals is observed. Moreover, one day after injection, an accumulation remains visible only in tumor area whereas in the whole tissue, the contrast is returned to initial level. This last result indicate a specific accumulation of the γFe_2O_3@PO-PEG-cRGD NPs on the tumor cells, revealing the glioma by MRI diagnosis.

4. Conclusion

Herein, we have described the synthesis of a new nanoplatform for the targeting of $\alpha_v\beta_3$ integrin over-expressed in brain tumors. In first step, iron oxide nanoparticles were surface functionalized with PO-PEG-COOH in order to improve their stability in biological media. In second step, the carboxylate end functions allowed to graft cRGD peptide with a ratio around 17 cRGD per nanoparticle under microwave conditions. In addition to their high transverse relaxivity (r_2 = 315 $mM^{-1} \cdot s^{-1}$), the γFe_2O_3@PO-PEG-cRGD NPs present good physic-chemical properties for circulation in the bloodstream up to brain vessels. The nanoplatform tends to accumulate in tumor tissue one day after injection indicating an active targeting induced by cRGD peptides onto NP surface. This proof-of-concept study allows considering this nanoplatform as a potential MRI contrast agent for glioblastoma diagnosis. The results presented here allow envisaging a new targeting tool more specific and efficient for the cancer diagnosis. A complete pharmacokinetic study will be performed to study the biodistribution of the NPs and identify the main clearance organs.

Author contributions

The manuscript was written through contributions of all authors. All authors have given approval to the final version of the manuscript

Transparency Document

The Transparency document associated with this article can be found, in online version.

References

[1] T.F. Massoud, S.S. Gambhir, Molecular imaging in living subjects: seeing fundamental biological processes in a new light, Genes Dev. 17 (2003) 545–580.
[2] M.A. Pysz, S.S. Gambhir, J.K. Willmann, Molecular imaging: current status and emerging strategies, Clin. Radiol. 65 (2010) 500–516.
[3] N. Grenier, P. Brader, Principles and basic concepts of molecular imaging, Pediatr. Radiol. 41 (2011) 144–160.
[4] R. Weissleder, Scaling down imaging: molecular mapping of cancer in mice, Nat. Rev. Cancer 2 (2002) 11–18.
[5] R. Weissleder, M.J. Pittet, Imaging in the era of molecular oncology, Nature 452 (2008) 580–589.
[6] M. Ferrari, Cancer nanotechnology: opportunities and challenges, Nat. Rev. Cancer 5 (2005) 161–171.
[7] R. Misra, S. Acharya, S.K. Sahoo, Cancer nanotechnology: application of nanotechnology in cancer therapy, Drug Discov. Today 15 (2010) 842–850.
[8] M. Chatel, M. Frenay, C. Lebrun, V. Bourg, F. Fauchon, Gliomes de haut grade: astrocytomes anaplasiques et glioblastomes, EMC – Neurol. 2 (2005) 257–278.
[9] M. Jhanwar-Uniyal, M. Labagnara, M. Friedman, A. Kwasnicki, R. Murali, Glioblastoma: molecular pathways, stem cells and therapeutic targets, Cancers 7 (2015) 538–555.
[10] L. Persano, E. Rampazzo, G. Basso, G. Viola, Glioblastoma cancer stem cells: role of the microenvironment and therapeutic targeting, Biochem. Pharmacol. 85 (2013) 612–622.
[11] T.A. Wilson, M.A. Karajannis, D.H. Harter, Glioblastoma multiforme: state of the art and future therapeutics, Surg. Neurol. Int. 5 (2014) 64.
[12] R.K. Jain, et al., Angiogenesis in brain tumours, Nat. Rev. Neurosci. 8 (2007) 610–622.

[13] S. Huang, et al., Tumor-targeting and microenvironment-responsive smart nanoparticles for combination therapy of antiangiogenesis and apoptosis, ACS Nano 7 (2013) 2860–2871.
[14] Z. Liu, F. Wang, X. Chen, Integrin α(v)β(3)-targeted cancer therapy, Drug Dev. Res. 69 (2008) 329–339.
[15] J.S. Desgrosellier, D.A. Cheresh, Integrins in cancer: biological implications and therapeutic opportunities. Nature reviews, Cancer 10 (2010) 9–22.
[16] M. Millard, S. Odde, N. Neamati, Integrin targeted therapeutics, Theranostics 1 (2011) 154–188.
[17] B. Estevez, B. Shen, X. Du, Targeting Integrin and Integrin Signaling in Treating Thrombosis, Arterioscler. Thromb. Vasc. Biol. 35 (2015) 24–29.
[18] S. Kaur, et al., Recent trends in antibody-based oncologic imaging, Cancer Lett. 315 (2012) 97–111.
[19] S. Richard, et al., Endothelin B receptors targeted by iron oxide nanoparticles functionalized with a specific antibody: toward immunoimaging of brain tumors, J. Mater. Chem. B 3 (2015) 2939–2942.
[20] F. Geinguenaud, I. Souissi, R. Fagard, Y. Lalatonne, L. Motte, Easily controlled grafting of oligonucleotides on γFe_2O_3 nanoparticles: physicochemical characterization of dna organization and biological activity studies, J. Phys. Chem. B 118 (2014) 1535–1544.
[21] F. Geinguenaud, I. Souissi, R. Fagard, L. Motte, Y. Lalatonne, Electrostatic assembly of a DNA superparamagnetic nano-tool for simultaneous intracellular delivery and in situ monitoring, Nanomed. Nanotechnol. Biol. Med. 8 (2012) 1106–1115.
[22] E. Ruoslahti, RGD and other recognition sequences for integrins, Annu. Rev. Cell Dev. Biol. 12 (1996) 697–715.
[23] K.K. Ganguly, S. Pal, S. Moulik, A. Chatterjee, Integrins and metastasis, Cell Adhes. Migr. 7 (2013) 251–261.
[24] E. Koivunen, B. Wang, E. Ruoslahti, Phage libraries displaying cyclic peptides with different ring sizes: ligand specificities of the RGD-directed integrins, Nat. Biotechnol. 13 (1995) 265–270.
[25] C. Mas-Moruno, F. Rechenmacher, H. Kessler, Cilengitide: the first anti-angiogenic small molecule drug candidate. design, synthesis and clinical evaluation, Anti Cancer Agents Med. Chem. 10 (2010) 753–768.
[26] V.A. Cuddapah, S. Robel, S. Watkins, H. Sontheimer, A neurocentric perspective on glioma invasion, Nat. Rev. Neurosci. 15 (2014) 455–465.
[27] G. Gambarota, W. Leenders, in: L. Schröder, C. Faber (Eds.), In vivo NMR imaging: methods and protocols, Humana Press 2011, pp. 477–487.
[28] J. Fang, H. Nakamura, H. Maeda, The EPR effect: unique features of tumor blood vessels for drug delivery, factors involved, and limitations and augmentation of the effect, Adv. Drug Deliv. Rev. 63 (2011) 136–151.
[29] Y. Lalatonne, et al., Mesoscopic structures of nanocrystals: collective magnetic properties due to the alignment of nanocrystals, J. Phys. Chem. B 108 (2004) 1848–1854.
[30] J. Bolley, et al., Carbodiimide versus click chemistry for nanoparticle surface functionalization: a comparative study for the elaboration of multimodal superparamagnetic nanoparticles targeting αvβ3 integrins, Langmuir 29 (2013) 14639–14647.
[31] J. Bolley, et al., Optimized multimodal nanoplatforms for targeting [small alpha]v[small beta]3 integrins, Nanoscale 5 (2013) 11478–11489.
[32] B.L. Frey, D.G. Hanken, R.M. Corn, Vibrational spectroscopic studies of the attachment chemistry for zirconium phosphonate multilayers at gold and germanium surfaces, Langmuir 9 (1993) 1815–1820.
[33] E. Teston, et al., Non-aqueous Sol–Gel synthesis of ultra small persistent luminescence nanoparticles for near-infrared in vivo imaging, Chem. Eur. J. 21 (2015) 7350–7354.
[34] E. Guénin, et al., Catechol versus bisphosphonate ligand exchange at the surface of iron oxide nanoparticles: towards multi-functionalization, J. Nanopart. Res. 16 (2014) 1–13.
[35] T.J. Daou, et al., Water soluble dendronized iron oxide nanoparticles, Dalton Trans. (2009) 4442–4449, http://dx.doi.org/10.1039/B823187G.